Electronic Supplementary Material (ESI) for Journal of Materials Chemistry C.

Supplementary Information

Synthesis of $CsPbBr_3$ Perovskite Nanocrystals with Acoustically Actuated Millisecond Mixing

Chun Kiu Ng,[a] Hao Deng,[b] Hanchen Li,[a] Wenping Yin,[a] Tuncay Alan*[b] and Jacek J. Jasieniak*[a]

[a] *ARC Centre of Excellence in Exciton Science, Department of Materials Science and Engineering, Faculty of Engineering, Monash University, Clayton, VIC 3800, Australia.*
[b] *Department of Mechanical and Aerospace Engineering, Laboratory for Microsystems, Faculty of Engineering, Monash University, Clayton, VIC 3800, Australia.*

Table of Contents

1. Generation of Cs_4PbBr_6
2. Microfluidic system mixing time calculation
3. Videography and integrated pixel color analysis of batch mixing process
4. Characterization of Relative Mixing Index
5. Microfluidic Platform Optimization Parameters
6. X-Ray Diffraction Sample Preparation
7. Time-Dependent Measurements
8. Isolation of Nanoplatelets
9. References

1. Generation of Cs_4PbBr_6

Preliminary experiments within a passive Y-junction PDMS microfluidic chip with a 0.040 M precursor solution saw significant generation of Cs_4PbBr_6. DMF is able to dissolve $CsPbBr_3$ crystals but cannot dissolve Cs_4PbBr_6. This is demonstrated in Figure S1 which shows blue emitting $CsPbBr_3$ nanoplatelets encapsulated within Cs_4PbBr_6 precipitates, which were unable to be removed from the channel after flushing with DMF and then with TOL. It was for this reason that DMSO was used which could successfully clean the channel of all generated crystals.

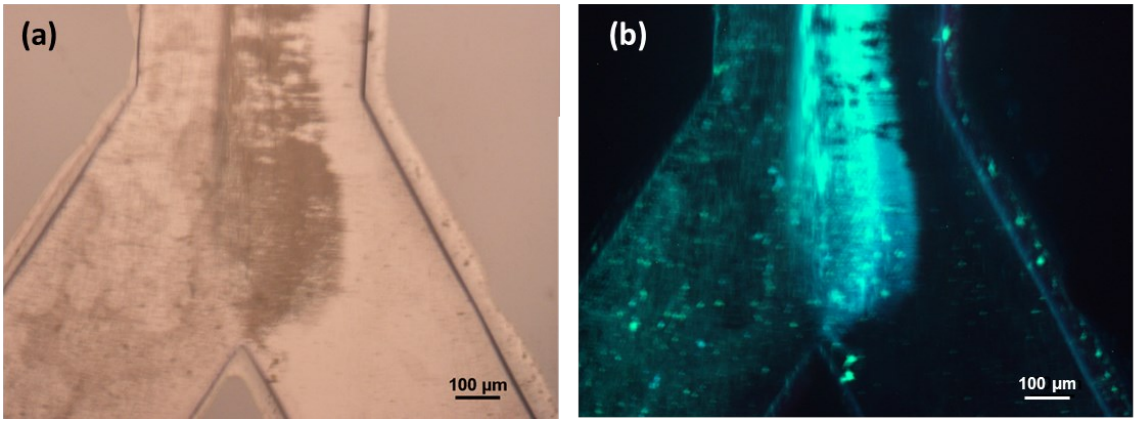

Figure S1. Micrograph of a Y-junction chip post-synthesis and after DMF and toluene flushing under (a) visible light and (b) UV light (λ = 395 nm).

Different batch-LARP reaction conditions were investigated under the usual DMF:TOL ratio of 1:10 with a precursor concentration of 0.040 M with a slow addition rate. With all concentrations kept constant, the inclusion/exclusion of OA and OLA, and their placement in DMF or toluene were briefly examined. It was found that the effects of ligands were more dominant on the reaction than the influence of DMF, with the standard batch LARP reaction with the ligands placed with the metal salts in DMF as ideal.

Sample 1: $(DMF + CsBr + PbBr_2) + OA + OLA \rightarrow Toluene$

Sample 2: $(DMF + CsBr + PbBr_2) + OA \rightarrow Toluene$

Sample 3: $(DMF + CsBr + PbBr_2) + OLA \rightarrow Toluene$

Sample 4: $(DMF + CsBr + PbBr_2) \rightarrow Toluene + OA + OLA$

Sample 5: $(DMF + CsBr + PbBr_2) \rightarrow Toluene + OA$

Sample 6: $(DMF + CsBr + PbBr_2) \rightarrow Toluene + OLA$

Sample 7: $(DMF + CsBr + PbBr_2) \rightarrow Toluene$

Moreover, crude dispersion Samples #1,2,5,7 in Figure see $CsPbBr_3$ undergo dissolution from DMF over time, which primarily results in micro-sized, non-fluorescent $CsPbBr_3$ crystals forming. For these samples, only Sample #1 (standard batch-LARP reference) contains any oleylamine/oleylammonium (OLA/OLA^+). Conversely, Samples #3,4,6 saw the clear dissolution and conversion of $CsPbBr_3$ to white Cs_4PbBr_6 precipitates, which all have the commonality of containing oleylamine/oleylammonium (OLA/OLA^+) and DMF being present. The presence of DMF is necessary in this conversion process as purified DMF-free $CsPbBr_3$ dispersions containing OLA/OLA^+ can remain stable for months, meaning that it is not solely dependent on the amine/ammonium. When these purified dispersions do degrade, only the formation of orange microcrystals is observed and not white Cs_4PbBr_6 precipitates.

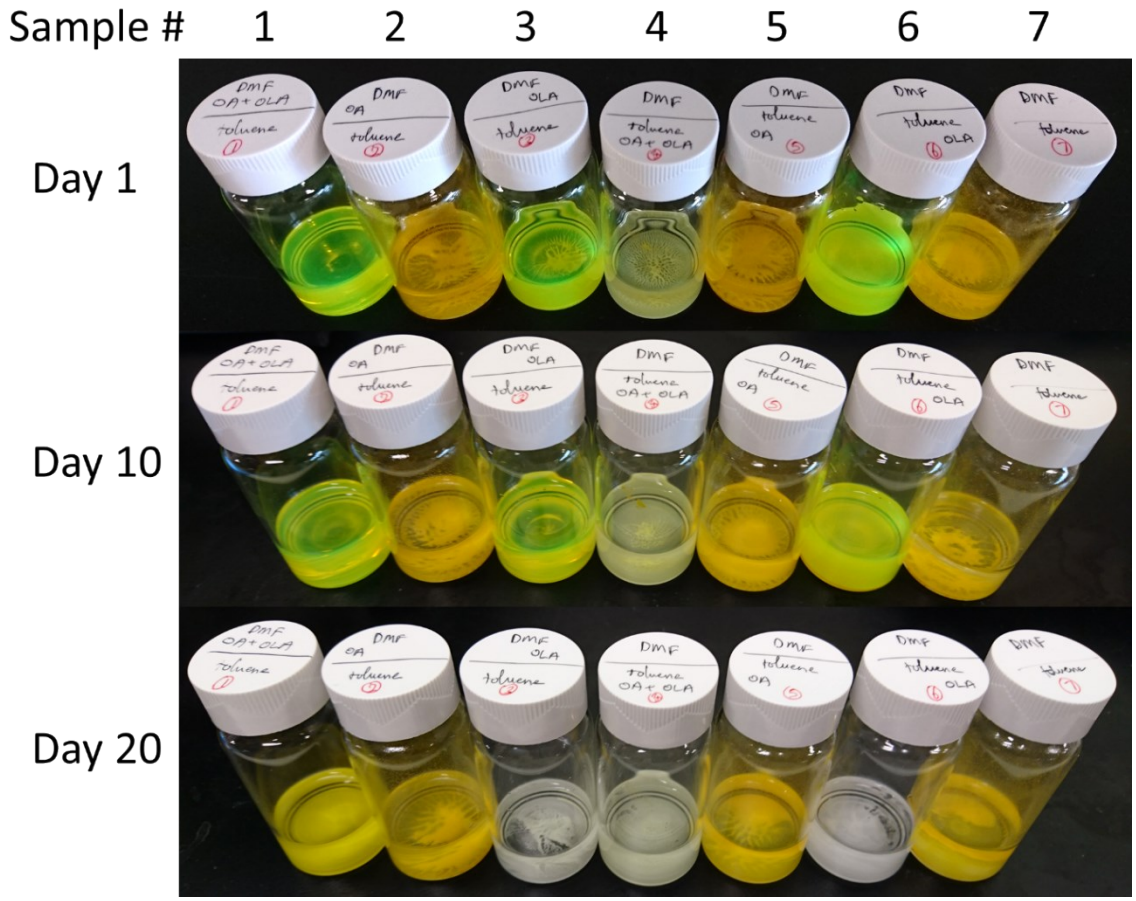

Figure S2. Different batch-LARP synthesis of $CsPbBr_3$ under different two-pot reaction conditions which were monitored over 3 weeks.

2. Microfluidic system mixing time calculation

The time required for the solution to be mixed homogeneously (t_{mixing}) is calculated by the equation below:

$$t_{mixing} = \frac{L_{mix}}{U}$$

where L_{mix} is the mixing length for homogenization, and U is the flow velocity. The two intersecting solutions are in an unmixed state at the bottom of the oscillating cantilevered structure and become homogeneously mixed by the time it reaches the top of the hole. As it is unknown at which point the solutions become homogeneous through the hole, this means that L_{mix} is therefore equal to or less than the thickness of the chip (500 ± 25 µm). The flow velocity is calculated by dividing the flowrate over the cross-sectional area. The time required to reach homogeneity is therefore estimated to be equal to or less than 23 ms at 1.1 mL/min flowrate. Further detail of the mixing time calculation is discussed in a previous publication.[1]

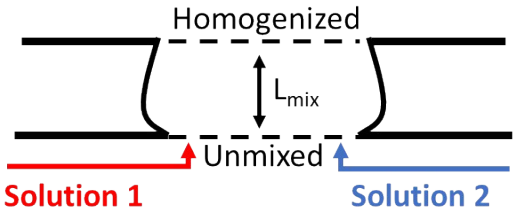

Figure S3. Schematic of the through hole region where the two streams of solutions are mixed by the oscillating cantilever.

3. Videography and integrated pixel color analysis of batch mixing process

To characterize the mixing condition in batch process, the process of injecting 1 mL of fluorescence dye into 10 mL of DI water that is being stirred by a magnetic stirrer were filmed in slow motion at 120 FPS (Supplementary Video S1.). The brightness deviation of pixels within the vial area were analyzed frame by frame using MATLAB (Figure S4). The pixel brightness deviation stabilized at 2.2 s after injection, indicating a 2.2 s mixing time.

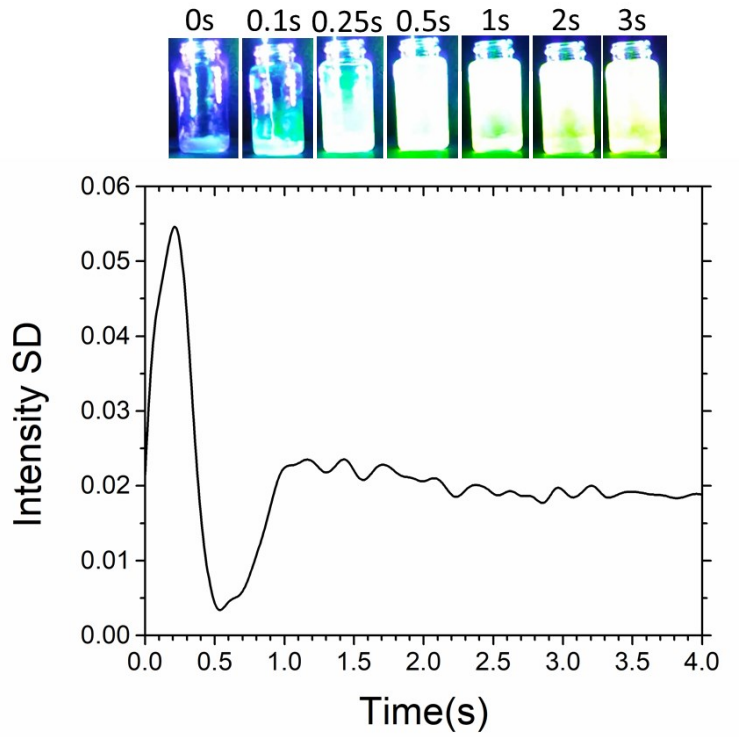

Figure S4. Pixel brightness intensity analysis of slow motion (120 FPS) video footage of 1 mL dye injected into 10 mL water under UV-light (λ = 395 nm), complete homogenization occurs 2.2 seconds after injection.

4. Characterization of Relative Mixing Index

To quantify the mixing performance, a water-dye mixing experiment has been conducted. Water is mixed with a fluorescent dye (Invitrogen Molecular Probes, Thermo Fisher Scientific, USA) with the same setup as used in the perovskite synthesis, and recorded by a digital camera (AM4023CT, Dino-lite Digital Microscope, TW) at 15 FPS. The frames corresponding to the mixed and unmixed condition are then selected and transformed into grayscale images. The standard deviation of the intensity of the pixels across the width of the channel for mixed (σ) and unmixed (σ_0) conditions are then calculated with Equation S1 and S2.

$$\sigma = \sqrt{\frac{1}{N}\sum_{i=1}^{N}\left(I_i - \langle I\rangle\right)^2} \quad \text{(S1)}$$

$$\sigma_0 = \sqrt{\frac{1}{N}\sum_{i=1}^{N}\left(I_{0i} - \langle I\rangle\right)^2} \quad \text{(S2)}$$

Where N denotes the number of pixels, $\langle I\rangle$ represents the average intensity of the pixels, and I_i is the local intensity of a pixel. The Relative Mixing Index (RMI), a dimensionless term that has often been used for assessing the mixing performance, compares the homogeneity before and after mixing. It is computed by comparing σ and σ_0 using Equation S3.[2]

$$RMI = 1 - \sigma/\sigma_0 \quad \text{(S3)}$$

Where 0 and 1 represent the worst and best mixing efficiencies respectively. Due to external factors such as nonuniform lighting, and dirt on the camera lens the RMI of 1 is not achievable. As a next step, to provide a more realistic description of mixing performance, we normalize RMI with the mixing index of a premixed solution. To perform the normalization, fluorescent dye and water are mixed thoroughly using a vortex mixer for 30 seconds (sufficient time for it to mix completely). This homogenized solution is then pumped through the channel, and its RMI (RMI_{100}) is computed. (The RMI_{100} should be measured right before or after each experiment to ensure they are

exposed to the same lighting and other external conditions). An RMI (RMI_N) is then calculated by normalizing RMI against RMI_{100}, with Equation S4.

$$RMI_N = RMI/RMI_{100} \quad \text{(S4)}$$

By performing this normalization step, the influence from the potential variables such as the lighting condition and other factors can be eliminated, allowing for more accurate and consistent measurement of the mixing performance.

5. Microfluidic Platform Optimization Parameters

Despite the 0.020 M precursor being partially opaque at room temperature, which is not ideal, it is homogeneous enough to be compatible with the microfluidic platform without too many major issues With the 0.020 M precursor, it is found that the lowest flow rate here of 0.55 mL/min was the only one to not possess adventitious Cs_4PbBr_6 (Figure 4a). This is attributed to the prolonged mixing time enhancing the homogenization of the partially precipitated OLA^+-OA^- salts in the precursor solution mitigating significant by-product formation. Conversely, the higher flow rates above 0.55 mL/min reduces the residence time through the oscillator and does not appear to be sufficiently long to homogenize the precursor solution, as evident by the presence of Cs_4PbBr_6. In the extreme case of 3.3 mL/min, the very short mixing time of 6 ms saw significant quantities of large Cs_4PbBr_6 crystals and mixed $CsPbBr_3$ morphologies of NPL and NCu that is reminiscent of the MF platform being used in its passive mode.

As stated previously, the ligands are only partially solubilized for precursor concentrations of 0.030 M and 0.040 M and results in an unexpected red shift against the expected trend. At 0.030 M, the non-solubilized ligand appears in a range of particulate sizes where most can still flow through the syringe tip and connection line to the micromixer. At 0.040 M, because of the higher fraction of non-solubilized ligand, the precursor solution contains a mixture of ligand salt particulates and flakes. It has been observed that due to their large size, flakes of non-solubilized ligand often accumulate near the neck of the syringe and are believed to act as a pseudo-filter which prevent other flakes and/or particulates of insolubilized ligand from exiting the syringe. This results in a lower ratio of 'ligand to metal salt' than intended being introduced to the micromixer at 0.040 M. This similarly applies to the 0.030 M samples but to a lesser extent and is absent in the 0.020 M and 0.010 M variants. From our previous experiments which have examined this phenomenon with an ethylacetate anti-solvent, where variable ligand concentrations were tested against a constant metal halide concentration, a red shifting trend was observed.[3] As ligands play a pivotal role in arresting growth and stabilizing the nanocrystals, the reduction in ligand content results in faster crystal growth. Therefore, the red shifted microfluidic platform spectra from the 0.040 M compared to 0.030 M results, for both active and passive mixing conditions are the result of a lower 'ligand to metal salt' ratio than intended. This effectively mimics a sample using a precursor concentration between 0.020-0.030 M if the proper 'ligand to metal salt' ratio.

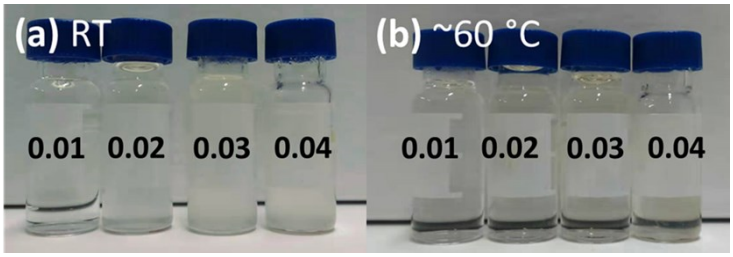

Figure S5. Different precursor concentrations at (a) room temperature where 0.010 M is transparent, 0.020 M is slightly opaque, 0.030 M and 0.040 M are very opaque. (b) When the solutions have been gently warmed to ~60 °C, all solutions become transparent as the ligand salts fully solubilize in DMF.

XRD measurements on the crude $CsPbBr_3$ nanocrystal solutions' crystal products were performed to gauge the relative fraction of Cs_4PbBr_6 present within the initial reaction mixtures. Figure S7 shows the XRD spectra of crude solutions made using a precursor concentration of 0.010 M for both batch (slow and fast addition rates) and microfluidic methodologies (1.37 W active and 0.0 W passive mixing). This shows that the MF platform sample with active mixing has significantly less Cs4PbBr6 than for the other three variants.

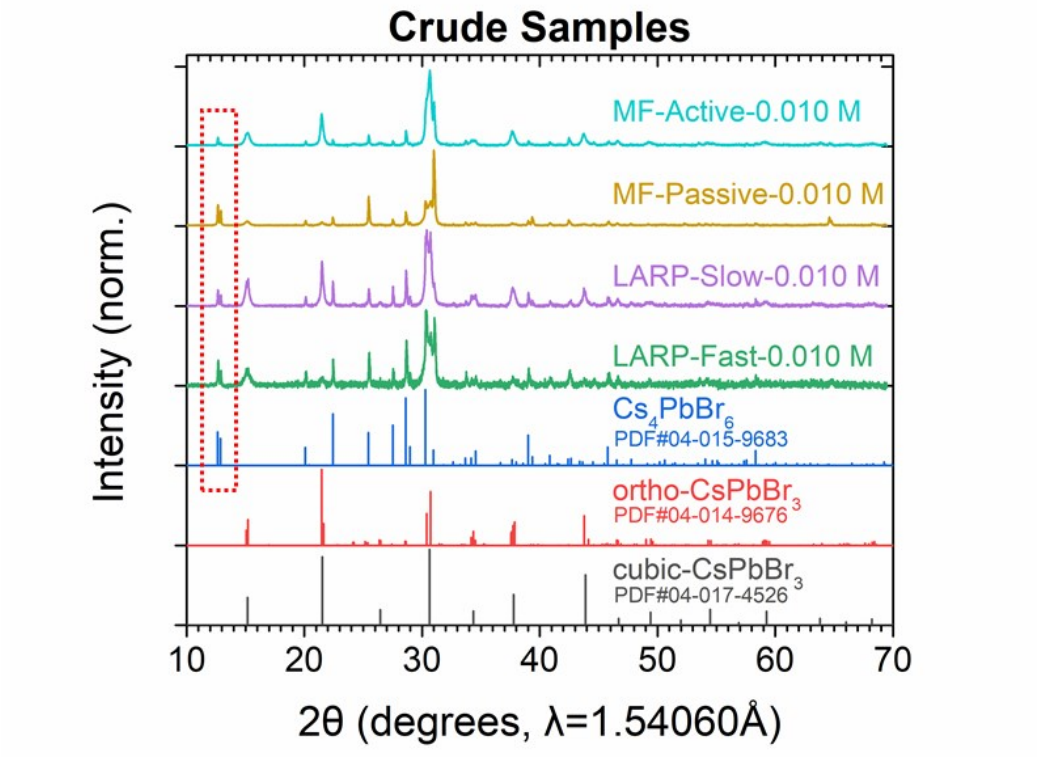

Figure S6. XRD spectra of the crude LARP solution's crystal products from both batch and MF based LARP methodologies, as well as reference spectra of their products. Dotted region shows the characteristic and unique Cs_4PbBr_6 doublet peak.

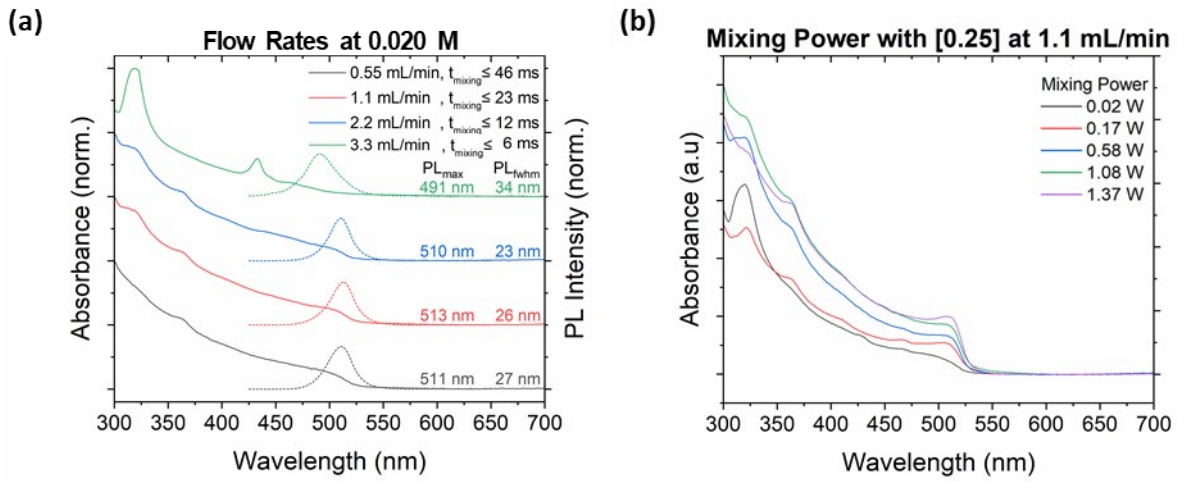

Figure S7. (a) UV-Vis (solid line) and PL (dotted line) spectra of $CsPbBr_3$ samples synthesized with the MF platform examining the dependence of the various flow rates operating with a precursor concentration of 0.010 M. (b) Absorbance measurements from Figure 4e with reduced scattering using FluorTools a|e Spectral Software's inbuilt function for a qualitative comparison on the differences in the band edge against different input powers. Note, the local maxima at 509 nm for 1.37 W's absorbance spectrum may be the result of larger non-colloidal nanocrystals which are also responsible for light scattering.

6. X-Ray Diffraction Sample Preparation

For analyzing the differently synthesized crude solutions, the perovskite and any perovskite-related products were fully precipitated into pellets via centrifugation to be dispersed in toluene (i.e. once washed). This prepared solution

was then deposited onto a soda-lime glass substrate and gently dried under flowing gas under ambient conditions. The films were then taken for XRD measurements under a rotation of 15 ° per second. For analyzing the purified $CsPbBr_3$ solutions, these were prepared as described in the main text and similarly deposited onto glass substrates as described above.

7. Time-Dependent Measurements

For the initial investigation on the impact of mixing on nucleation and growth in a batch LARP synthesis, time-dependent PL measurements were taken from a synthesis conducted within a cuvette cell. A cuvette was filled with 3.0 mL of toluene with 10 µL of the 0.040 M precursor injected and measured with the Horiba spectrometer. The precursor is carefully injected into the center of the cuvette with minimal induced turbidity by the injection stream. In the absence of magnetic stirring, NPL possessing different thicknesses are initially observed, with the most dominant PL peak centered at ~440 nm being characteristic of two-unit cell thick NPL (Figure S8a).[4] Over time, these progressively transform into thicker NCu, as evidenced by the gradual redshift of the PL peak that is initially centered at ~475 nm. Notably, even after 10 mins, the growth of these NCu has not reached completion, which is consistent with an Ostwald ripening mechanism.[5] In contrast, when mixing is applied, the growth process completed within 45 s and remained unchanged after 5 min of standing (Figure S8b).

To better gauge when the growth process is complete, the measurement was repeated as above using a StellarNet spectrometer capable of magnetic stirring at 2000 rpm (Figure S8c,d). Under continuous mixing and shorter spectral requisition times, this revealed that the PL peak position stabilized in ~10 s, indicating an end to PNC growth. This is corroborated with secondary measurements on a standard LARP reaction volume, using slow motion videography and integrated pixel color analysis under λ = 395 nm UV-light, showing the pixel's green component mirroring the PL peak position evolution (Figure S8e,f, Supplementary Video S2), which is correlated with the PNC size.[6] This demonstrates the importance of mixing in obtaining homogeneous $CsPbBr_3$ NCu, with the absence or poor mixing resulting in prolonged growth processes with mixed morphologies. For the slow-motion videography analysis, one droplet of precursor (~35 µL) is added to 10 mL of vigorously stirred toluene under λ = 365 nm UV-light and recorded with a Google pixel G-2PW4200 android phone back camera at 240 FPS (Supplementary Video S2). The pixel analysis is performed by averaging the RGB values of all pixels in the selected area for each frame and filtered with a low-pass filter for noise reduction.

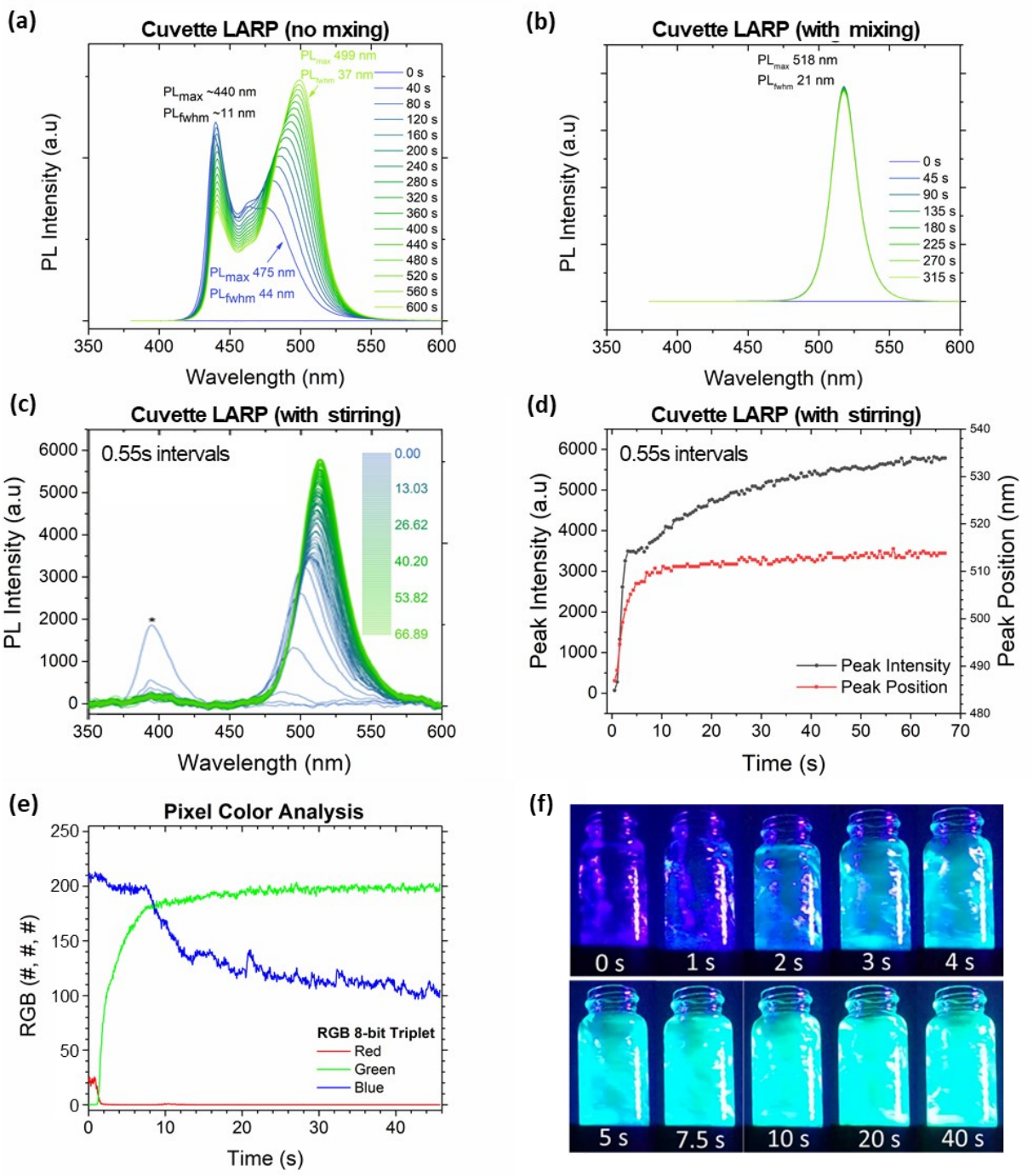

Figure S8. (a) Time-dependent PL spectra of $CsPbBr_3$ PNCs solutions made within a cuvette with (a) no mixing and (b) with mixing measured on a Horiba spectrometer. (c) In-situ time-dependent photoluminescence measurements of the LARP reaction with active mixing, and (d) its PL peak intensity and peak position evolution plotted against time; '*'marks reflections from the 400 nm LED light source. (e) Pixel color analysis of slow-motion video footage of the LARP reaction under UV-light (λ = 395 nm), with the injection occurring at the ~2 s mark, with near immediate fluorescence indicating the formation of $CsPbBr_3$ and mostly stabilizing after ~10 s of reaction time. (f) Corresponding photographs of the reaction mixture under UV-light (λ = 395 nm) at different reaction times.

The same StellarNet benchtop spectrometer system was used to obtain the data for the in-situ batch-LARP spectra in Figure S8c,d was attempted for the microfluidic synthesis. Unfortunately, in-situ time dependent measurements were challenging with the present setup, as the relatively low signal-to-noise ratio did not allow reliable time-resolved data to be collected. Therefore, aliquots of different growth times (0.020 M precursor under 1.37 W active mixing) by

controlling the tubing length was devised to achieve time-dependent measurements with ethyl acetate as a quenchant, with a final crude:quenchant ratio of 1:3. To show that this approach to quench crystal growth was effective in the microfluidic system, Figure a shows the microfluid quenched samples, as well as an unquenched sample with the shortest growth time of 0.12 s within the microfluidic system that was not previously shown. Due to our experimental setup, across all the samples a 1 minute lag was present. Because of this factor, even when the aliquot was taken for measurement at the shortest growth time of 0.12 s within the microfluidic platform, without quenching the continued crystal growth results in $CsPbBr_3$ nanocuboids with an absorption that did not change over one hour of ambient ageing. In contrast, for a quenched sample, an initially observed population of $CsPbBr_3$ NPLs, with an absorption peak at 445 nm, is consumed to concurrently grow nanocuboids. This is evident from the gradual redshift of the absorption onset of the quenched samples with longer growth/flow times before being quenched. The small absorption peak at ~470 nm corresponds to a population of $CsPbBr_3$ nanocubes which are ~6.6 nm in size, with higher wavelength absorption peaks indicating a larger crystal size.[6] While there is an underlying question on the role of ethyl acetate in the final product, if the quenching process was ineffective, then all the quenched spectra should be near identical and would be representative of nanocuboids due to large scale precipitation. This is clearly not the case. Moreover, ethyl acetate has not been observed to act as an etching agent in our experience. If it were, there would likely be an increased intensity in NPL peaks and a blueshift in the absorption onset which is not observed. Both of these factors suggest that ethyl acetate acts as a benign solvent which can sufficiently slow crystal growth to gauge the evolution in their absorption. This is demonstrated in Figure S10b where it shows quenched samples with the same 0.12 s growth time within the microfluidic system, but measured with a 1 min and ~30 min lag time between sample collection and measurement. Since ethyl acetate drives colloidal instability, it is believed that this slows further crystal growth from Ostwald ripening and/or oriented attachment after nucleation – which with the micromixer should be near instantaneous. If there is an influence from using ethyl acetate to quench the crude solution, steps were taken to minimize it as much as possible and would be a systematic error in the measured spectra for Figure S10a. There is the small possibility that the formation of nanoplates may be the result of unreacted precursors nucleating when exposed to ethyl acetate and were not originally formed when mixed with toluene. Attempts to elucidate the true origin of the nanoplatelets have so far been inconclusive due to the short time frames in which they seem to exist.

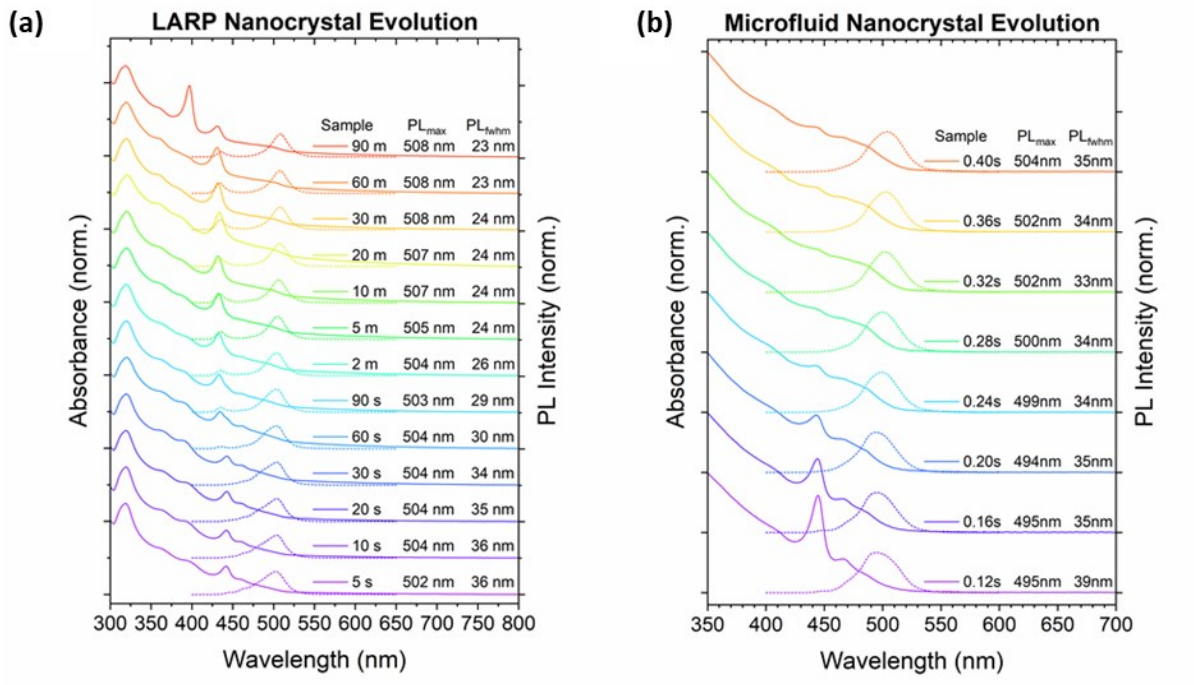

Figure S9. (a) Time dependent UV-Vis and PL spectra of a LARP fast injection reaction at a concentration of 0.040 M, (b) and with the microfluid platform examining <0.5 second growth times at a concentration of 0.020 M under active (1.37 W) mixing.

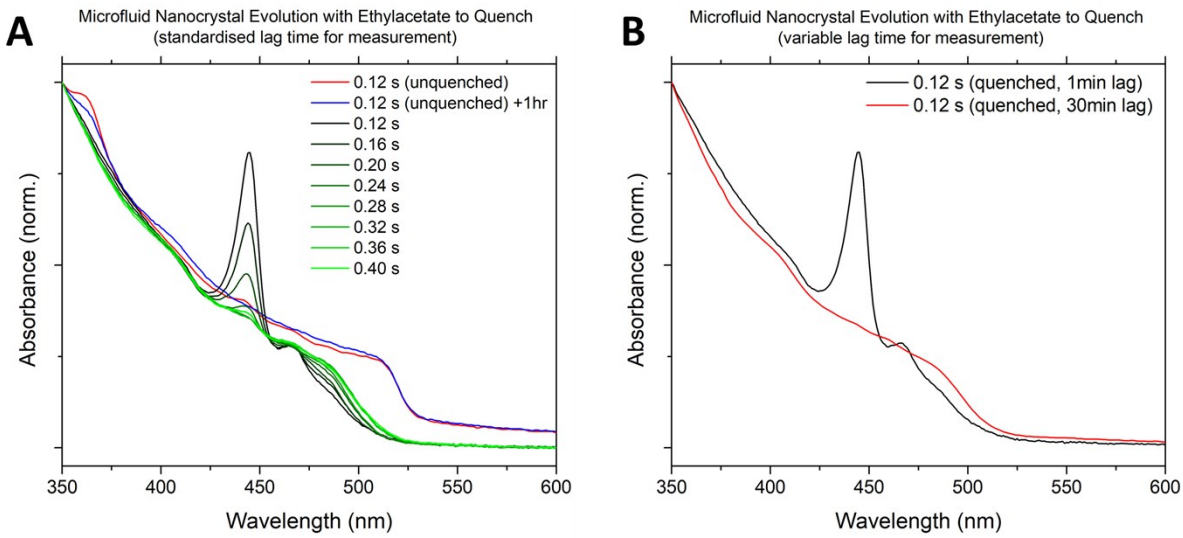

Figure S10. (a) UV-Vis spectra of the microfluidic nanocrystal evolution data presented in the manuscript's Figure 5d with the addition of an unquenched sample at the shortest growth time of 0.12 s within the microfluidic platform. For this latter sample, we provide two sets of data, one that was taken after 1 minute of sample collections (i.e. our minimum time between collection and measurement) and after 1 hour of ageing. (b) UV-Vis spectra of the microfluidic nanocrystal evolution of two quenched samples with identical growth times within the microfluidic system but with different lag times, i.e. delay time between sample collection and sample measurement.

8. Isolation of Nanoplatelets

Figure shows the absorption spectra of the crude, supernatant and precipitated material, during an attempt to isolate the initial population of nanoplatelets in the crude showing a strong absorption peak at 414 nm. However, all attempts were unsuccessful, as the optical characterizations suggests that the nanoplatelets converted into nanocubes, underwent dissolution or damaged during centrifugation. Based on these difficulties, TEM of these samples proved inconclusive because it was not possible to isolate the nanoplatelets for TEM during purification without affecting their original morphology.

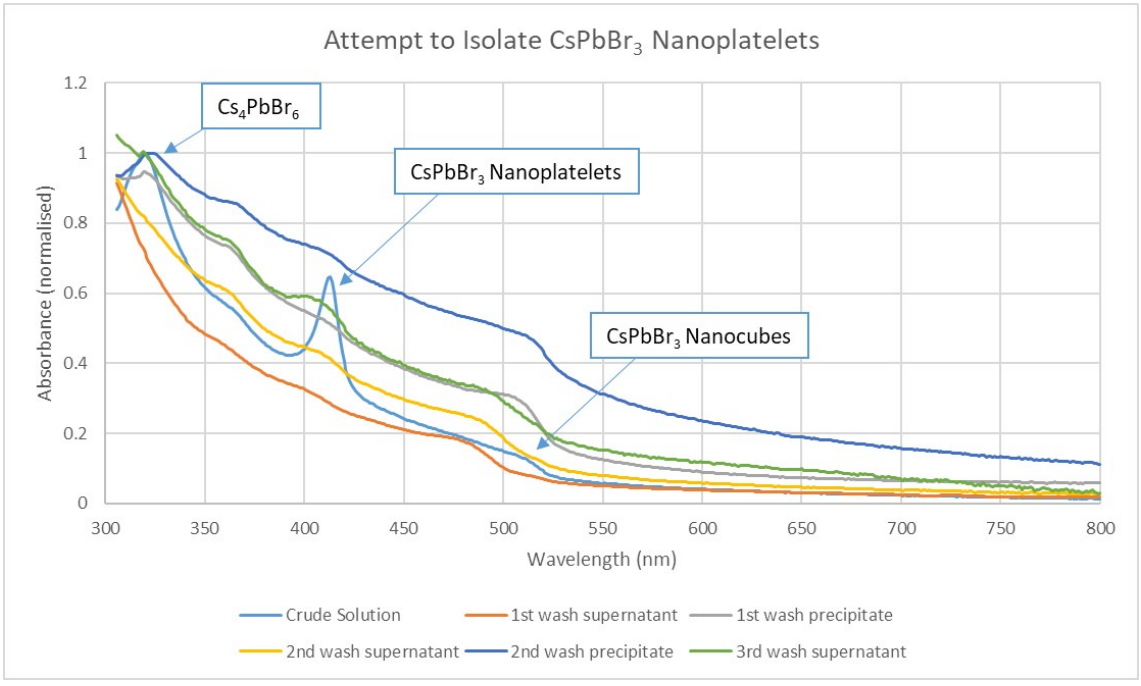

Figure S11. UV-Vis absorption spectra of a crude $CsPbBr_3$ dispersion with three distinct phases, and resultant supernatant and precipitated material while attempting to isolate the nanoplatelets.

9. References

1 N. H. An Le, H. Deng, C. Devendran, N. Akhtar, X. Ma, C. Pouton, H. K. Chan, A. Neild and T. Alan, *Lab Chip*, 2020, **20**, 582–591.

2 A. Hashmi and J. Xu, *J. Lab. Autom.*, 2014, **19**, 488–491.

3 C. K. Ng, W. Yin, H. Li and J. J. Jasieniak, *Nanoscale*, 2020, **12**, 4859–4867.

4 Y. Bekenstein, B. A. Koscher, S. W. Eaton, P. Yang and A. P. Alivisatos, *J. Am. Chem. Soc.*, 2015, **137**, 16008–16011.

5 M. Koolyk, D. Amgar, S. Aharon and L. Etgar, *Nanoscale*, 2016, **8**, 6403–6409.

6 L. Protesescu, S. Yakunin, M. I. Bodnarchuk, F. Krieg, R. Caputo, C. H. Hendon, R. X. Yang, A. Walsh and M. V. Kovalenko, *Nano Lett.*, 2015, **15**, 3692–3696.